

# Functional MRI of the Lung

Y. Berthezène\*

Hôpital de la Croix Rousse, Service de Radiologie, Laboratoire Creatis-LRMN CNRS - UMR 5220- U 630 Inserm, 103, Grande rue de la Croix Rousse, 69317 Lyon Cedex 04, France

**Abstract:** Imaging of the pulmonary parenchyma represents a unique challenge for MRI. Limited signal is caused by low proton density, susceptibility artefacts, and physiological motion (cardiac pulsation, respiration). Improvements in MRI techniques have extended the potential for investigations of pulmonary parenchymal disease with the evaluation of lung perfusion. More recently inhalation of non proton-MRI nuclei such as hyperpolarized gases ( $^3\text{He}$  or  $^{129}\text{Xe}$ ) can provide functional ventilation images.

**Keywords:** Lung diseases, pulmonary function, lung MRI, lung ventilation, lung perfusion.

## INTRODUCTION

While proton-MRI has emerged in the past few years as a technique of choice for imaging many organs and diseases, lung parenchyma still remains one of the most difficult tissues to be imaged because of three main factors:

- The low density of air-filled lung parenchyma, resulting in low proton density and weak NMR signal intensity
- The important motion artefacts due to physiological displacements (cardiac and respiratory motions);
- Susceptibility effects induced by multiple air and tissue interfaces which cause many local gradients responsible for very low values of T2.

Several strategies have been developed to overcome these difficulties. Image acquisition during breathhold or using respiratory gating and/or EKG triggering procedures results in reduced motion artefacts and a fixed position of the diaphragm and the cardiac cavities during image reconstruction. Susceptibility artefacts can be minimized by the use of spin echo sequences and very short echo-time. Nonetheless, the weak NMR signal remains the major drawback for lung MRI. In this context, the development of new contrast agents is of crucial importance for increasing the NMR signal from the lung. Extra cellular or strictly intravascular contrast agents administered intravenously (Gd chelates) have been used to enhance lung parenchyma and evaluate lung perfusion. Beside proton MRI, other nuclei can be used for MRI. They include Helium-3, Xenon-129 and Fluorine-19.<sup>3</sup>He and <sup>129</sup>Xe are inert gases, and they can be applied easily by inhalation.

## PROTON IMAGING

Low spin density is the major drawback for MRI of the lung, especially for the visualization of normal lung

parenchyma and of lung diseases with loss of tissue such as emphysema. It can be approached by the use of gradient-echo sequences with short repetition times, low flip angle, a higher number of acquisitions and large voxels. In many lung diseases, the amount of tissue, fluid and/or cells is increased by the pathological process. Thus, a higher number of protons are accessible, and significant improvements of the SNR can be achieved. To make use of the higher spin density short echo times are important to avoid signal loss from T2 relaxation [1]. However, in various cases such a disease related increase of spin density is not sufficient for accurate delineation, characterization and diagnosis of the disease process. Paramagnetic contrast agents have the potential to increase the MR signal from the lungs when using very short echo times which reduce susceptibility effects arising from air-tissue interfaces. They are used for enhancement of nodules or consolidations, for MR angiography or for perfusion imaging.

## Chronic Infiltrative Lung Disease

In Chronic infiltrative lung disease, the pathology itself induces an increase in proton density and a reduction of susceptibility artefacts [2]. Alveolitis demonstrates high signal intensity on T1w and T2w images and also shows manifest enhancement after contrast administration. Signal intensity correlated with clinical severity of disease and potential response to therapy. Successful anti-inflammatory treatment decreasing the activity of alveolitis or development of fibrosis in the natural course of the disease are associated with a decrease in signal intensity. King *et al.* have shown that, the administration of a contrast agent significantly improved the detection of honeycombing but not the detection of ground-glass opacities [3]. Although, extent and distribution of airspace disease is clearly depicted at MRI, it is still inferior to CT regarding anatomic assessment and demonstration of fibrosis, i.e. parenchymal bands and reticular abnormalities [5]. In animals, macromolecular contrast agents may improve the differentiation between alveolitis and fibrosis even further [6]. In the active alveolitic phase, leakage of macromolecules from the intravascular into the extravascular compartment was observed. In the fibrotic phase, enhancement was markedly diminished which

\*Address correspondence to this author at the Hôpital de la Croix Rousse, Service de Radiologie, Laboratoire Creatis-LRMN CNRS - UMR 5220- U 630 Inserm, 103, Grande rue de la Croix Rousse, 69317 Lyon Cedex 04, France; Tel: 33 4 72 07 18 80; Fax: 33 4 72 07 18 86; E-mail: yves.berthezene@creatis.univ-lyon1.fr

indicates a decrease in plasma volume within the fibrotic lung [6]. Macromolecular contrast agents will greatly improve the assessment of the inflammatory alveolitic processes in the future.

### **Pulmonary Edema**

Magnetic resonance imaging has also been used successfully to evaluate the lung water content qualitatively and quantitatively [7]. These properties can be used to characterize the microvascular barrier function within the lung. In hydrostatic pulmonary edema in rats, the T1 relaxation time was significantly longer than in normal controls, whereas T2 relaxation time was not different. In permeability pulmonary edema, however, T1 and T2 relaxation times were significantly longer than in normal controls [8]. It could also be demonstrated that T1 and T2 are linearly related to extravascular lung water in an induced permeability edema in rats [9]. In normal excised pig lungs, a 95% correlation between MR measurements and gravimetric lung water content was found [10]. Using a three-dimensional gradient-echo sequence which is sensitive to water the entire lung can be covered with a spatial and temporal resolution sufficient to observe the development of pulmonary edema in an experimentally induced acute respiratory distress syndrome [11]. The results indicate that edema formation can be imaged regionally and quantified globally estimating the mismatch of transcapillary filtration flow and lymph clearance [12].

Lung water sequences were also successfully applied in humans. Measurements of average lung density were easily performed. Lung intensity decreased with full inspiration. It gives an estimate of regional lung expansion. Regional measurements of lung density are used to determine lung density gradients. These gradients did not show a significant change in the prone or the supine position. From the calculated lung density gradients, pleural pressure gradients can be calculated. They also decrease with full inspiration. In normal volunteers, MR measurements of these parameters were similar to those obtained with more invasive procedures [10]. Edema and infiltrative lung disease increase lung density and decrease the elastic properties of the lung, and MR measurements of lung water content may prove useful in the assessment of parenchymal lung disease. In animal models, using macromolecular contrast media, pulmonary edema of different etiologies (increased vascular pressure *vs* damaged capillary barriers) can be separated [13]. Measurements of the total intravascular volume using macromolecular contrast agents and the determination of total lung water using a multi-spin-echo sequence allow for an accurate calculation of extravascular lung water. There was a high correlation with gravimetric reference measurements in the quantitation of pulmonary edema.

Although some approaches are ready to use, MRI of pulmonary edema has not been established in clinical routine.

### **Perfusion**

There are several different approaches to image lung perfusion. Some of them are based on spin tagging techniques, called Flow sensitive Alternating Inversion Recovery (FAIR) and FAIR with an extra radiofrequency

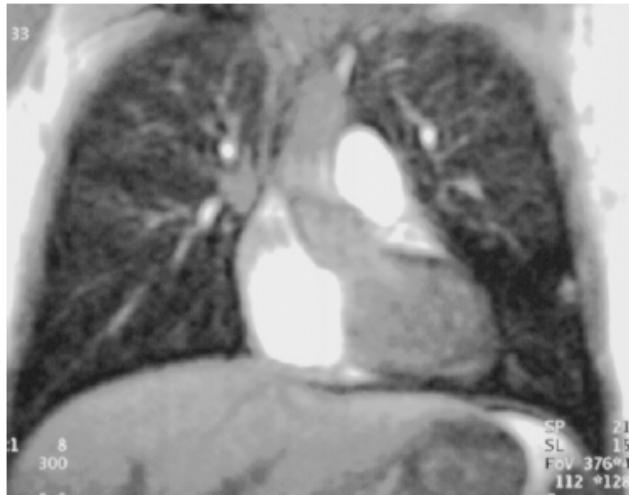
pulse (FAIRER). The blood water is magnetically labeled and used as an endogenous, freely diffusible tracer. With inversion times of 1000-1500 ms enhancement of the lung parenchyma and the peripheral pulmonary vessels down to the subsegmental level was observed [14]. The classical method requires the administration of intravenous contrast agent (Gd-chelates) to evaluate lung perfusion. Gd-chelates will reduce the longitudinal relaxation (T1) of blood resulting in an increase in signal intensity. Usually, imaging is performed during the first pass of the contrast agent through the lung using a fast imaging sequence with a short TE to reduce susceptibility artefacts.

Changes of signal intensity during the first passage are detected with inversion recovery 2D turbo-FLASH with ultrashort TE or 3D FISP with short TR and short TE [15, 16]. For both techniques, the non-enhanced images are subtracted from the enhanced images, such as in digital subtraction angiography. The final image is a selective perfusion map of the lung. For the 2D sequence time-intensity curves were calculated to assess the time course of perfusion [17]. From the 3D FISP acquisition maximum intensity projection of perfusion were generated and assessed visually [18]. These techniques were successfully used to detect perfusion defects in patients with pulmonary embolism [19] (Fig. 1a). In a prospective comparative study with perfusion lung scintigraphy, perfusion MRI had an average sensitivity of 69% and specificity of 91% for the detection of perfusion defects. The overall agreement between MR and scintigraphy appeared to be good ( $\kappa_{0.63}$ ) [20]. MR perfusion imaging was also capable to demonstrate physiological preferences of pulmonary perfusion. The gravity-dependence of lung perfusion was observed in volunteers who were investigated in supine and prone position [21]. In patients after single lung transplantation, preferred perfusion of the dorsal parts of the lung in supine position was clearly demonstrated by a higher increase in signal intensity [22]. These preliminary data in patients suggest that perfusion imaging might be quite helpful in the diagnosis of pulmonary embolism. It remains unclear whether perfusion imaging will provide clinically helpful information on perfusion defects and heterogeneity in emphysema or chronic infiltrative lung disease.

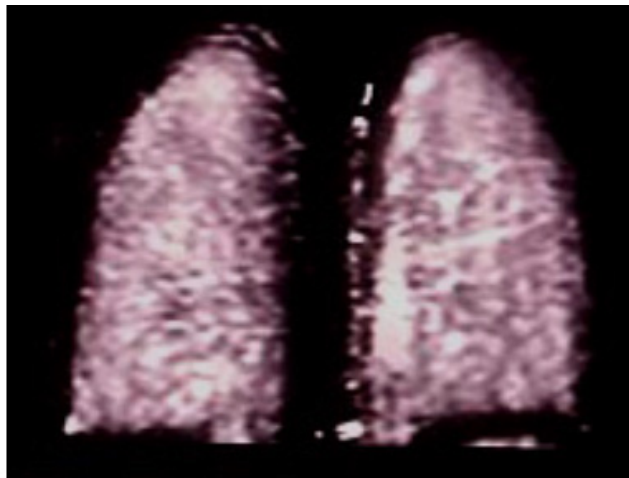
### **Oxygen-Enhanced Lung MRI**

The use of 100% oxygen as a paramagnetic contrast agent in MR imaging of the lung was first proposed by Edelman, Chen and Stock [23-25]. A shortening of the T1 of the lung parenchyma on the order of 100-200 ms (10%) was reported during breathing 100% oxygen, resulting in a signal intensity variation on the order of 20% on optimized T1-weighted sequences (Fig. 1b). The optimum dosage for 100% O<sub>2</sub> was shown to be 15 L/min [26]. Administration of 100% oxygen with this dosage has been shown to produce oxygen concentrations in the lung of 60-80% [27]. Above 15 L/min, a plateau in signal intensity increase was observed. Several investigators have suggested that prolonged hyperoxia due to 100% oxygen inhalation can cause diffuse alveolar damage and lung fibrosis [27]. Such noxious effects were observed on animal experiments and occurred during prolonged hyperoxia of several hours or days, whereas in O<sub>2</sub>-enhanced MRI lung studies, hyperoxia lasts less than 1 h in total and is alternated with periods of normoxia. MR images

are acquired with the subjects in a supine position alternately inhaling room air and 100% oxygen using a non-rebreathing ventilation mask or a mouthpiece associated with a nose clamp. A typical O<sub>2</sub> inhalation paradigm consists of subjects alternately breathing room air for about 1 min and 100% oxygen for about 2 min. The difference between the images of the two states yields the oxygen-enhanced ventilation images. Ventilation maps can be expressed as the percentage of relative enhancement. Image acquisition can be triggered either right after the air/O<sub>2</sub> switch for assessment of wash-in or washout or about 120 s after the switch to allow static imaging.



a



b

**Fig. (1).** Patient with a suspected pulmonary embolism. Gadolinium perfusion image demonstrates a perfusion defect in the left lower lobe (a). Oxygen coronal ventilation image demonstrates a homogeneous lung enhancement (b).

Simultaneous cardiac and respiratory synchronization has been shown to improve image quality [28] with a reduced variability of signal intensity and diaphragm mismatch. Image acquisition can be performed during quiet breathing, at the end of expiration when the signal intensity is higher (due to higher proton density and smaller susceptibility effects) as compared with acquisition at full inspiration. Only short suspensions of breathing of less than 3 s are

required during acquisition, which is especially important for patients who could have difficulties in holding their breath at end-expiration.

Several studies aimed to compare signal intensity changes or signal intensity time course with DLCO, standard pulmonary function tests, HRCT or scintigraphy in healthy volunteers and patients with pathologic diffusive capacity such as idiopathic lung fibrosis or emphysema [27, 29]. In patients, mean enhancement ratio was significantly lower and signal intensity time course showed a delayed signal intensity increase [27, 29]. Weak and heterogeneous enhancement of 10-26% was found in patients with pulmonary emphysema [27]. Regional differences that correlated with findings on radiographs and CT scans were seen on the signal intensity slope and on the maps of signal intensity change. Enhancement was excellently correlated with DLCO [27] and strongly correlated with HRCT emphysema score. Mean upslope of enhancement calculated from dynamic acquisitions was strongly correlated with forced expiratory volume in 1 s (FEV1) and had a good to excellent correlation with DLCO [29]. A prospective study in 30 patients with lung cancer, showed that post-surgical FEV1 and predicted oxygen enhanced MRI FEV1 was excellently correlated [27].

### HYPERPOLARIZED GASES

Compared with conventional water proton imaging, MRI of gases is inherently limited by the much lower spin density of the gas phase (typically three orders of magnitude drop in spin density).

One effective way to circumvent the low NMR sensitivity of gases is to acquire MR signal from the so-called hyperpolarized (HP) or laser-polarized gases.

Among other parameters, the NMR signal-to-noise ratio (SNR) per unit volume is depending linearly on the polarization level  $P$ , defined as the percentage of the maximum achievable nuclear macroscopic magnetization of the sample. For the nuclei of the atoms of interest in biomedical NMR (hydrogen, fluorine, phosphorus, sodium, etc), the value of the polarization level at thermal equilibrium, the so-called Boltzmann polarization level, is in the order of a few parts per million (ppm). However, nuclear polarization high above thermal equilibrium can be achieved by the use of appropriate polarization techniques. The polarization levels can be typically increased by 5 orders of magnitude compared with the Boltzmann equilibrium level, resulting in a similar increase in detectable NMR signal.

### MR Imaging Using HP 3He and 129Xe

The large NMR signal offered by HP gases allows one to image their distribution in the pulmonary tree and the alveolar spaces. The first NMR biomedical application of HP 129Xe was reported in 1994 with intrapulmonary space imaging of excised mouse lungs [31]. The first *in vivo* animal lung ventilation images obtained using HP 3He were reported one year later [32] followed by the first human lung images [33, 34]. Imaging of the intrapulmonary distribution of HP gases can be used for the visualization of ventilated airspaces. The spatial resolution of lung ventilation images obtained using 3He exceed by an order of magnitude the spatial resolution that are routinely obtained with

scintigraphy techniques using radioactive gases. In human studies, typical spatial resolution in the millimeter range are reported (Fig. 2), while in rodents studies sub-millimetric resolution (Fig. 3) is usually reached [36]. Spatial resolution obtained with  $^{129}\text{Xe}$  ventilation images is typically 3 to 5 times lower due to reduced available SNR. Physical and chemical interactions of the HP gases with their biological environment can be advantageously exploited for obtaining structural or functional information on the lungs. The most commonly used physical parameters are the diffusion length, the longitudinal relaxation times, the velocity, the flow and the chemical shift of the HP gases.

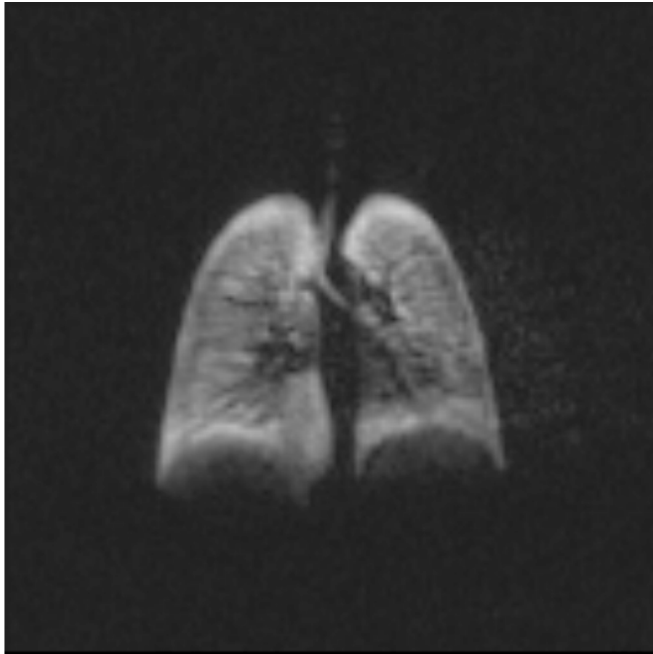


**Fig. (2).** Coronal hyperpolarized  $^3\text{He}$  gas MR image in a normal volunteer.

MR diffusion imaging is a well known technique applied essentially for measuring the so-called apparent diffusion coefficient (ADC) of water in tissues. The ADC values of HP gases in airspaces depend on gas composition (dilution of HP gases in pulmonary gases) and above all on the restriction of gas atoms diffusion by the broncho-alveolar walls. The diffusion length of helium atoms during typical diffusion sensitizing times (a few milliseconds) exceeds the diameter of alveolar sacks (a few hundreds of micrometers). Hence, in the time scale of MR acquisition,  $^3\text{He}$  diffusion in alveolar space takes place in a restricted regime. The dependence of HP gases ADC values upon the dimensions of the alveolar space can be used as a non-invasive tool for probing the lung architecture at a sub-pixel level. Indeed,  $^3\text{He}$  ADC values have been shown to significantly increase in patients with emphysema compared with healthy volunteers [37]. These  $^3\text{He}$  ADC changes in emphysematous lungs are attributed to morphological changes in alveolar structure and more specifically to airspace enlargements that characterize emphysema [37-40]. The longitudinal relaxation time,  $T_1$ , of  $^3\text{He}$  in the lung is approximately 20 s. The relaxation rate  $R_1$  of  $^3\text{He}$  is varying linearly with the partial pressure of oxygen due to dipolar interactions of  $^3\text{He}$  nucleus with paramagnetic molecular oxygen [41].

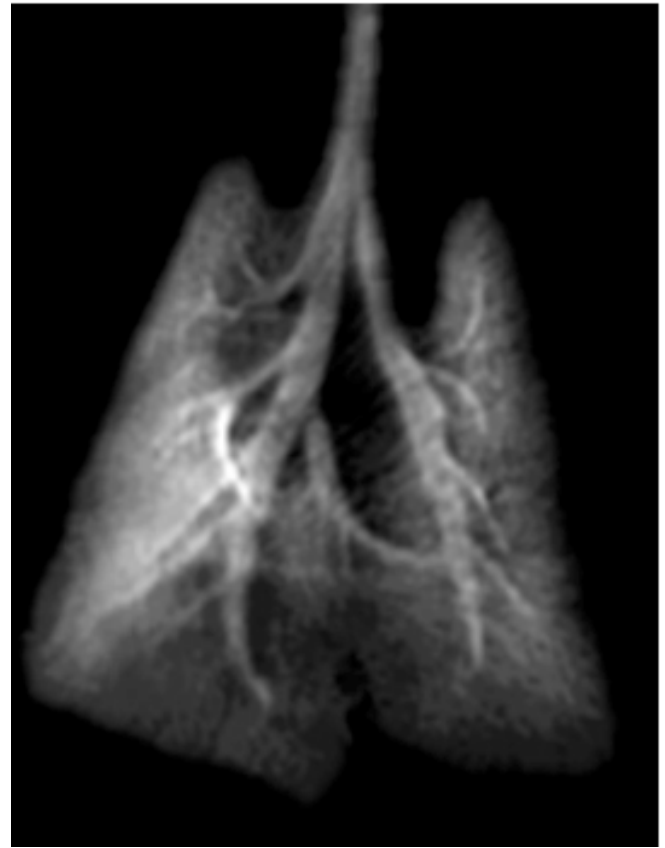


**Fig. (3).** Coronal 3D hyperpolarized  $^3\text{He}$  gas MR image in a normal rat.

By measuring the time variation of the relaxation time of HP  $^3\text{He}$  in the lungs, it is then possible to compute locally the alveolar oxygen concentration and the consumption rate of oxygen *in vivo* [42,43] (Fig. 4). The velocity of HP gas in the lungs can be measured from velocity-encoded MR imaging sequences and HP gases lung inflow or outflow can be derived from dynamic ventilation image series [44]. Among other applications, these dynamic gas MRI techniques have been used in animal models for the evaluation of bronchoconstrictive drug effects [45] and in clinical studies following lung transplant in patients [46]. Chemical shift imaging has been demonstrated using HP  $^{129}\text{Xe}$ . The high solubility and the large chemical shift (several hundreds of ppm) of xenon allow one to differentiate between xenon in alveoli and xenon dissolved in tissue. The so-called xenon polarization transfer contrast (XTC) technique aims to probe the xenon exchange between alveolar space and blood/tissue compartments [47]. The method is based on the selective destruction of xenon polarization in lung parenchyma. Owing to the rapid exchange of xenon between the gas and the tissue phase, the depolarization of xenon dissolved in tissue affects the xenon signal from the gaseous phase. Using an appropriate pixel-based signal analysis of this effect, the authors obtained so-called XTC lung images with a contrast related to the exchange rate of xenon between the tissue and the alveolar space. A similar approach, called CSSR (chemical shift saturation recovery) was recently demonstrated and applied in human studies to investigate the alveolar surface area per unit volume of gas [48]. Besides ventilation imaging, HP gas imaging has been applied for the assessment of tissue perfusion, the acquisition of

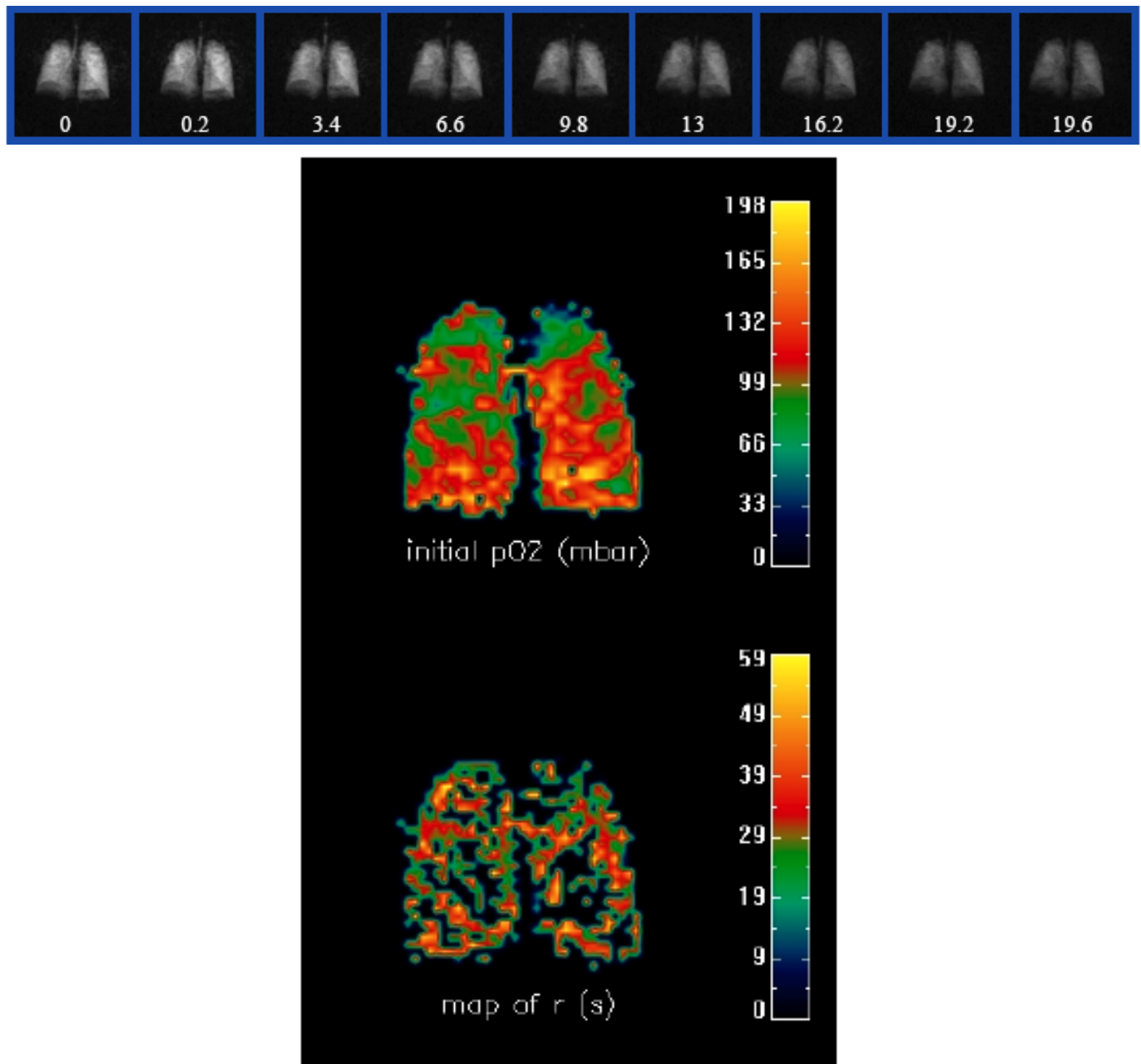


**Fig. (4).** The relaxation rate  $R_1$  of  $^3\text{He}$  is varying linearly with the partial pressure of oxygen due to dipolar interactions of  $^3\text{He}$  nucleus with paramagnetic molecular oxygen (top). Alveolar oxygen concentration and consumption rate of oxygen in a volunteer (bottom).

angiographic images and the characterization of biological tissues. These applications of HP gases have been restricted so far essentially to pre-clinical studies.

#### Preclinical Examinations

Emphysema disease in animal models has been extensively studied using  $^3\text{He}$  and  $^{129}\text{Xe}$  MRI. Elastase-induced emphysema has been investigated in rat [38, 40], mouse [49] and rabbit [50] using  $^3\text{He}$  or  $^{129}\text{Xe}$  diffusion MRI. Measurements performed at end-expiratory inflation volume demonstrated an increase by 20% of ADC values in the lungs of elastase-treated animals compared with ADC values in healthy control animals [38]. When measurements were carried out at total lung capacity,  $^3\text{He}$  ADC values increased from 0.15  $\text{cm}^2/\text{s}$  in normal rats to 0.18  $\text{cm}^2/\text{s}$  in

elastase-challenged animals; moreover, a significant correlation was found between the  $^3\text{He}$  ADC values and the alveolar internal area assessed by histology in lungs fixed with formalin at an airway pressure corresponding to the total lung capacity [40]. Similarly,  $^3\text{He}$  ADC values averaged over the entire lungs were found to be approximately 25% higher in emphysema mice than in healthy animals [35].

As mentioned previously, it is possible to compute the alveolar partial pressure of oxygen, ( $p\text{O}_2$ ) *in vivo* from the relaxation time of the HP  $^3\text{He}$  in the lungs. As the intrapulmonary oxygen partial pressure distribution is governed by local ventilation, perfusion and  $\text{O}_2$  uptake,  $p\text{O}_2$  assessment can be used to evaluate lung function. As a matter of fact, the determination of  $p\text{O}_2$  values and of their

time evolution during breathhold represents an indirect measure of the ventilation/perfusion ratio. The potential of  $^3\text{He}$  imaging for detecting perfusion abnormalities based on  $\text{pO}_2$  measurement was demonstrated in an experimental pig model [51]. After isolated pulmonary arterial occlusion using a balloon catheter, a focal T1 reduction corresponding to an abnormally high  $\text{pO}_2$  (related to the absence of perfusion) was observed, which normalized upon deflation of the balloon. More recently,  $\text{pO}_2$  imaging and oxygen depletion rate imaging was extended to small animal studies in rats and mice [52,53]. The potential of  $^3\text{He}$  MRI for assessing airways constriction has been demonstrated in methacholine-induced bronchoconstriction in rat models [45]. Using a Cine-MRI approach in which image acquisition was synchronized with the inhalation of the gas mixture ( $^3\text{He}$  with oxygen and nitrogen), heterogeneously distributed airways constriction was observed, resulting in a partition of the lung between ventilated and non-ventilated regions. The diameter of the main airways decreased by approximately 11% following methacholine injection. In a methacholine-induced broncho-constriction rat model [45], dynamic ventilation image series obtained from a single breath were used to generate parametric pixel-by-pixel maps of gas arrival time, filling time constant, inflation rate and gas volume and to assess these parameters in distal areas of the lung. Quantitative and regional analysis of gas flow, volume and arrival time demonstrated statistically significant differences between the baseline and constricted states. These differences were attributed to constriction of peripheral airways.

### Clinical Applications

Longitudinal studies or follow-up examinations for treatment or therapy monitoring are limited by the ionizing nature of the standard clinical imaging techniques (radiography, CT or scintigraphy). HP gases imaging represents a relevant diagnostic modality when multiple examinations are required for improving the patient management care. Up to now, the clinical applications of HP gases have been focused mainly on the investigation of three lung diseases: emphysema, cystic fibrosis and asthma.

In clinical studies, the regional measurement of  $^3\text{He}$  ADC values has been used to evaluate the severity of emphysema in patients [54-56]. This approach is supported by the good correlation observed between the  $^3\text{He}$  ADC values and alveolar dimensions [40]. Additionally, the  $^3\text{He}$  ADC values have been shown to correlate with spirometric indexes such as FEV1 (forced expiratory volume in 1 second) in healthy volunteers and in emphysema patients [57].  $^3\text{He}$  imaging has been also applied for the investigation of young patients (children and adolescent) with cystic fibrosis. Since the radiation exposure experienced in case of ionizing imaging modalities is problematic for children,  $^3\text{He}$  MRI represents an interesting alternative to standard imaging technique.  $^3\text{He}$  MRI has been demonstrated to be well suited for the visualization of ventilation defects (Fig. 5) and for evaluation of the efficacy of therapies such as physical therapies or bronchodilator inhalation [58-60]. Asthma disease is characterized by the inflammation and the obstruction of small airways. Several studies have investigated and demonstrated the potential of HP  $^3\text{He}$  in clinical studies with asthmatic patients [61-63]. It has been

shown that small and reversible ventilation defects that characterize asthma can be detected using HP  $^3\text{He}$  and that the efficiency of bronchodilator and physical challenge can be locally assessed. Furthermore, the variations in airflow obstructions as depicted with  $^3\text{He}$  MRI correlate with the clinical evaluation of asthma severity and spirometry measurements.

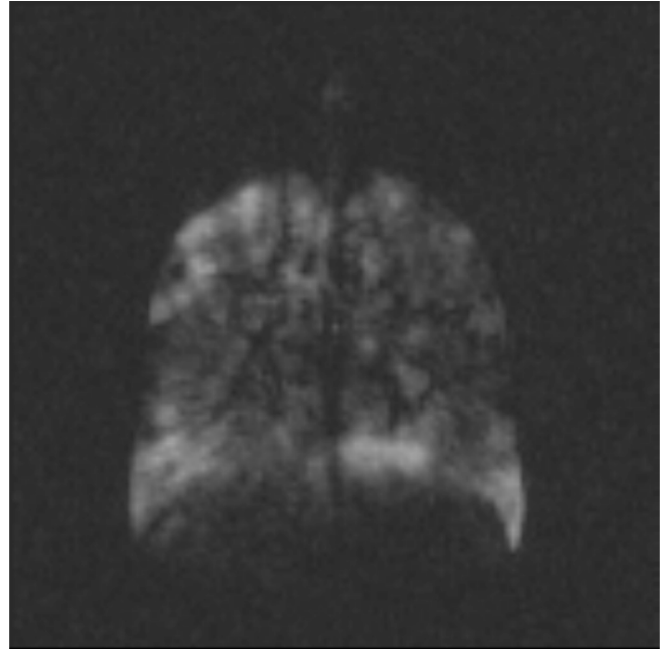


**Fig. (5).** Coronal hyperpolarized  $^3\text{He}$  gas MR image in a patient with cystic fibrosis with multiple ventilation defects.

### CONCLUSION

CT plays a major role in the imaging approach to structure and function in ARDS. CT has an impact on the optimization of the ventilatory strategies. However, great improvement has been made in MRI of the pulmonary parenchyma during the past years. The lung will not remain the forgotten organ for MR imaging in the future. Promising research activities are under way to introduce functional MRI of the lung. MRI will offer visualization of lung morphology as well as functional assessment of ventilation and pulmonary perfusion in a single examination.

### REFERENCES

- [1] Bergin C, Glover G, Pauly J. Lung parenchyma: magnetic susceptibility in MR imaging. *Radiology* 1991; 180: 845-8.
- [2] Müller N, Mayo J, Zwirowich C. Value of MR imaging in the evaluation of chronic infiltrative lung disease: comparison with CT. *Am J Roentgenol* 1992; 158: 1205-9.
- [3] King M, Bergin C, Ghadishah E, Yi E, Clark J. Detecting pulmonary abnormalities on magnetic resonance images in patients with usual interstitial pneumonitis: effects of varying window settings and gadopentetate dimeglumine. *Acad Radiol* 1996; 3: 300-7.
- [4] Matsumoto S, Mori H, Miyake H, *et al.* MRI signal characteristics of progressive massive fibrosis in silicosis. *Clin Radiol* 1998; 53: 510-4.
- [5] Kalaitzoglou I, Drevelengas A, Palladas P, Asimaki A. MRI appearance of pulmonary Wegener's granulomatosis with concomitant splenic infarction. *Eur Radiol* 1998; 8: 367-70.
- [6] Berthezène Y, Vexler V, Kuwatsuru R, *et al.* Differentiation of alveolitis and pulmonary fibrosis with a macromolecular MR imaging contrast agent. *Radiology* 1992; 185: 97-103.

- [7] Carroll F, Lloyd J, Nolop K, Collins J. MR imaging parameters in the study of lung water. *Invest Radiol* 1985; 20: 381-7.
- [8] Schmidt H, Tsay D-G, Higgins C. Pulmonary edema: a MR study of permeability and hydrostatic types in animals. *Radiology* 1986; 158: 297-302.
- [9] Skalina S, Kundel H, Wolf G, Marshall B. The effect of pulmonary edema on proton nuclear magnetic resonance relaxation times. *Invest Radiol* 1984; 19: 7-9.
- [10] Mayo J, MacKay A, Whittall K, Baile E, Paró P. Measurement of lung water content and pleural pressure gradient with magnetic resonance imaging. *J Thorac Imaging* 1995; 10: 73-81.
- [11] Caruthers S, Paschal C, Pou N, Harris T. Relative quantification of pulmonary edema with noncontrast-enhanced MRI. *J Magn Reson Imaging* 1997; 7: 544-50.
- [12] Caruthers S, Paschal C, Pou N, Roselli R, Harris T. Regional measurements of pulmonary edema by using magnetic resonance imaging. *J Appl Physiol* 1998; 84: 2143-53.
- [13] Berthezène Y, Vexler V, Jerome H, Sievers R, Moseley M, Brasch R. Differentiation of capillary leak and hydrostatic pulmonary edema with a macromolecular MR imaging contrast agent. *Radiology* 1991; 181: 773-7.
- [14] Edelman R, Siewert B, Adamis M, Gaa J, Laub G, Wielopolski P. Signal targeting with alternating radiofrequency (STAR) sequences: application to MR angiography. *J Magn Reson Med* 1994; 31: 233-8.
- [15] Ohno Y, Murase K, Higashino T, *et al.* Assessment of bolus injection protocol with appropriate concentration for quantitative assessment of pulmonary perfusion by dynamic contrast-enhanced MR imaging. *J Magn Reson Imaging* 2007; 25: 55-65.
- [16] Eichinger M, Puderbach M, Fink C, *et al.* Contrast-enhanced 3D MRI of lung perfusion in children with cystic fibrosis-initial results. *Eur Radiol* 2006; 16: 2147-52.
- [17] David V, Chen Q, Goldfarb J, Levin D, Edelman R. Comprehensive diagnosis of pulmonary embolism using MR imaging. *Radiology* 1997; 201: 411-2.
- [18] Adam G, Neuerburg J, Spüntrup E, Mühler A, Scherer K, Günther R. Gd-DTPA-cascade-polymer: potential blood pool contrast agent for MR imaging. *J Magn Reson Imaging* 1994; 4: 462-6.
- [19] Marchal G, Bosmans H, Hecke P, Jiang Y, Aerts P, Bauer H. Experimental Gd-DTPA polylysine enhanced MR angiography: sequence optimization. *J Comput Assist Tomogr* 1991; 15: 711-5.
- [20] Berthezène Y, Vexler V, Price D, Wisner-Dupon J, Moseley M, Aicher K, Brasch R. Magnetic resonance imaging detection of an experimental pulmonary perfusion deficit using a macromolecular contrast agent. Polylysine-gadolinium-DTPA40. *Invest Radiol* 1992; 27: 346-51.
- [21] Stock K, Chen Q, Levin D, Hatabu H, Edelman R. Demonstration of gravity-dependent lung perfusion with contrast-enhanced magnetic resonance imaging. *J Magn Reson Imaging* 1999; 9: 557-61.
- [22] Berthezène Y, Croisille P, Bertocchi M, Houzard C, Bendib K, Revel D. Lung perfusion demonstrated by contrast-enhanced dynamic magnetic resonance imaging: application to unilateral lung transplantation. *Invest Radiol* 1997; 32: 351-6.
- [23] Edelman RR, Hatabu H, Tadamura E, Li W, Prasad PV. Noninvasive assessment of regional ventilation in the human lung using oxygen-enhanced magnetic resonance imaging. *Nat Med* 1996; 2: 1236-9.
- [24] Chen Q, Jakob PM, Griswold MA, Levin DL, Hatabu H, Edelman RR. Oxygen enhanced MR ventilation imaging of the lung. *MAGMA* 1998; 7: 153-61.
- [25] Stock KW, Chen Q, Morrin M, Hatabu H, Edelman RR. Oxygen-enhanced magnetic resonance ventilation imaging of the human lung at 0.2 and 1.5 T. *J Magn Reson Imag* 1999; 9: 838-41.
- [26] Mai VM, Liu B, Li W, Polzin J, Kurucay S, Chen Q, Edelman RR. Influence of oxygen flow rate on signal and T(1) changes in oxygen-enhanced ventilation imaging. *J Magn Reson Imag* 2002; 16: 37-41.
- [27] Ohno Y, Hatabu H, Takenaka D, Van Cauteren M, Fujii M, Sugimura K. Dynamic oxygen enhanced MRI reflects diffusing capacity of the lung. *J Magn Reson Med* 2002; 47: 1139-44.
- [28] Molinari F, Gaudino S, Fink C, *et al.* Simultaneous cardiac and respiratory synchronization in oxygen-enhanced magnetic resonance imaging of the lung using a pneumotachograph for respiratory monitoring. *Invest Radiol* 2006; 41: 476-85.
- [29] Müller CJ, Schwaiblmair M, Scheidler J, *et al.* Pulmonary diffusing capacity: assessment with oxygen-enhanced lung MR imaging preliminary findings. *Radiology* 2002; 222: 499-506.
- [30] Ohno Y, Hatabu H, Higashino T, *et al.* Oxygen-enhanced MR imaging: correlation with postsurgical lung function in patients with lung cancer. *Radiology* 2005; 236: 704-11.
- [31] Albert MS, Cates GD, Driehuis B, *et al.* Biological magnetic resonance imaging using laser-polarized <sup>129</sup>Xe. *Nature* 1994; 370: 199-201.
- [32] Middleton H, Black RD, Saam B, *et al.* MR imaging with hyperpolarized <sup>3</sup>He gas. *J Magn Reson Med* 1995; 33: 271-5.
- [33] Ebert M, Grossmann T, Heil W, *et al.* Nuclear magnetic resonance in humans using hyperpolarized helium-3. *Lancet* 1996; 347: 1297-9.
- [34] MacFall JR, Charles HC, Black RD, *et al.* Human lung air spaces: potential for MR imaging with hyperpolarized He-3. *Radiology* 1996; 200: 553-8.
- [35] Viallon M, Cofer GP, Suddarth SA, *et al.* Functional MR microscopy of the lung with hyperpolarized <sup>3</sup>He. *J Magn Reson Med* 1999; 41: 787-92.
- [36] Chen BT, Yordanov AT, Johnson GA. Ventilation-synchronous magnetic resonance microscopy of pulmonary structure and ventilation in mice. *J Magn Reson Med* 2005; 53: 69-75.
- [37] Saam BT, Yablonskiy DA, Kodibagkar VD, *et al.* MR imaging of diffusion of (<sup>3</sup>)He gas in healthy and diseased lungs. *J Magn Reson Med* 2000; 44: 174-9.
- [38] Chen XJ, Hedlund LW, Möller HE, Chawla MS, Maronpot RR, Johnson GA. Detection of emphysema in rat lungs by using magnetic resonance measurements of <sup>3</sup>He diffusion. *Proc Natl Acad Sci USA* 2000; 10: 11478-81.
- [39] Yablonskiy DA, Sukstanskii AL, Leawoods JC, *et al.* Quantitative *in vivo* assessment of lung microstructure at the alveolar level with hyperpolarized <sup>3</sup>He diffusion MRI. *Proc Natl Acad Sci* 2002; 99: 3111-6.
- [40] Peces-Barba G, Ruiz-Cabello J, Cremillieux Y, *et al.* Helium-3 MRI diffusion coefficient: correlation to morphometry in a model of mild emphysema. *Eur Respir J* 2003; 22: 14-9.
- [41] Saam B, HapperW, Middleton H. Nuclear relaxation of <sup>3</sup>He in the presence of O<sub>2</sub>. *Phys Rev A* 1995; 52: 862-5.
- [42] Eberle B, Weiler N, Markstaller K, *et al.* Analysis of intrapulmonary O(2) concentration by MR imaging of inhaled hyperpolarized helium-3. *J Appl Physiol* 1999; 87: 2043-52.
- [43] Wild JM, FICHELE S, Woodhouse N, Paley MN, Kasuboski L, van Beek EJ. 3D volume-localized pO<sub>2</sub> measurement in the human lung with <sup>3</sup>He MRI. *J Magn Reson Med* 2005; 53: 1055-64.
- [44] Dupuich D, Berthezène Y, Clouet PL, Stupar V, Canet E, Cremillieux Y. Dynamic <sup>3</sup>He imaging for quantification of regional lung ventilation parameters. *J Magn Reson Med* 2003; 50: 777-83.
- [45] Mosbah K, Cre'millieux Y, Adeleine P, *et al.* Quantitative measurements of regional lung ventilation using helium-3 MRI in a methacholine-induced bronchoconstriction model. *J Magn Reson Imag* 2006; 24: 611-16.
- [46] Gast KK, Puderbach MU, Rodriguez I, *et al.* Distribution of ventilation in lung transplant recipients: evaluation by dynamic <sup>3</sup>He-MRI with lung motion correction. *Invest Radiol* 2003; 38: 341-8.
- [47] Ruppert K, Brookeman JR, Hagspiel KD, Mugler JP 3rd. Probing lung physiology with xenon polarization transfer contrast (XTC). *J Magn Reson Med* 2000; 44: 349-57.
- [48] Patz S, Muradian I, Hrovat MI, *et al.* Human pulmonary imaging and spectroscopy with hyperpolarized (<sup>129</sup>)Xe at 0.2 T. *Acad Radiol* 2008; 15: 713-27.
- [49] Dugas JP, Garbow JR, Kobayashi DK, Conradi MS. Hyperpolarized (<sup>3</sup>)He MRI of mouse lung. *J Magn Reson Med* 2004; 52: 1310-7.
- [50] Mata JF, Altes TA, Cai J, *et al.* Evaluation of emphysema severity and progression in a rabbit model: a comparison of hyperpolarized He-3 and <sup>129</sup>Xe diffusion MRI with lung morphometry. *J Appl Physiol* 2006; 102: 1273-80.
- [51] Jalali A, Ishii M, Edvinsson JM, *et al.* Detection of simulated pulmonary embolism in a porcine model using hyperpolarized <sup>3</sup>He MRI. *J Magn Reson Med* 2004; 51: 291-8.
- [52] Cieslar K, Stupar V, Canet-Soulas E, Gaillard S, Cremillieux Y. Alveolar oxygen partial pressure and oxygen depletion rate

- mapping in rats using  $(3)\text{He}$  ventilation imaging. *J Magn Reson Med* 2007; 57: 423-30.
- [53] Cieslar K, Alsaïd H, Stupar V, *et al.* Measurement of nonlinear  $\text{pO}_2$  decay in mice lungs using  $3\text{He}$ -MRI. *NMR Biomed* 2007; 20: 383-91.
- [54] Ley S, Zaporozhan J, Morbach A, *et al.* Functional evaluation of emphysema using diffusion-weighted  $3\text{He}$ -magnetic resonance imaging, high-resolution computed tomography, and lung function tests. *Invest Radiol* 2004; 39: 427-34.
- [55] Swift AJ, Wild JM, Fischele S, *et al.* Emphysematous changes and normal variation in smokers and COPD patients using diffusion  $3\text{He}$  MRI. *Eur J Radiol* 2005; 54: 352-8.
- [56] Fain SB, Panth SR, Evans MD, *et al.* Early emphysematous changes in asymptomatic smokers: detection with  $3\text{He}$  MR imaging. *Radiology* 2006; 239: 875-83.
- [57] Salerno M, de Lange EE, Altes TA, *et al.* Emphysema: hyperpolarized helium 3 diffusion MR imaging of the lungs compared with spirometric indexes - initial experience. *Radiology* 2002; 222: 252-60.
- [58] Donnelly LF, MacFall JR, McAdams HP, *et al.* Cystic fibrosis: combined hyperpolarized  $3\text{He}$ -enhanced and conventional proton MR imaging in the lung - preliminary observations. *Radiology* 1999; 212: 885-9.
- [59] Altes TA, de Lange EE. Applications of hyperpolarized helium-3 gas magnetic resonance imaging in pediatric lung disease. *J Magn Reson Imag* 2003; 14: 231-6.
- [60] Mentore K, Froh DK, de Lange EE, Brookeman JR, Paget-Brown AO, Altes TA. Hyperpolarized  $3\text{He}$  MRI of the lung in cystic fibrosis: assessment at baseline and after bronchodilator and airway clearance treatment. *Acad Radiol* 2005; 12: 1423-9.
- [61] Altes TA, Powers PL, Knight-Scott J, *et al.* Hyperpolarized  $3\text{He}$  MR lung ventilation imaging in asthmatics: preliminary findings. *J Magn Reson Imag* 2001; 13: 378-84.
- [62] Samee S, Altes T, Powers P, *et al.* Imaging the lungs in asthmatic patients by using hyperpolarized helium-3 magnetic resonance: assessment of response to methacholine and exercise challenge. *J Allergy Clin Immunol* 2003; 111 : 1205-11.
- [63] de Lange EE, Altes TA, Patrie JT, *et al.* Evaluation of asthma with hyperpolarized helium-3 MRI: correlation with clinical severity and spirometry. *Chest* 2006; 130: 1055-62.

---

Received: December 9, 2009

Revised: January 12, 2010

Accepted: January 12, 2010

© Y. Berthezène; Licensee *Bentham Open*.

This is an open access article licensed under the terms of the Creative Commons Attribution Non-Commercial License (<http://creativecommons.org/licenses/by-nc/3.0/>) which permits unrestricted, non-commercial use, distribution and reproduction in any medium, provided the work is properly cited.